

The Dynamics of the Radiated Field Near a Mobile Phone Connected to a 4G or 5G Network

Delia-Bianca Deaconescu
Doctoral School of Electrical Engineering
Technical University of Cluj-Napoca
Cluj-Napoca, Romania
deliadeaconescu@yahoo.com

David Vatamanu
Nicolae Balcescu Land Forces Academy
Lucian Blaga University
Sibiu, Romania
davidvatamanu@yahoo.com

Andreea Maria Buda
Nicolae Balcescu Land Forces Academy
Politehnica University of Bucharest
Bucharest, Romania
budaandreea98@yahoo.com

Simona Miclaus
Dept. Communications, IT & Cyb. Def.
Nicolae Balcescu Land Forces Academy
Sibiu, Romania
simo.miclaus@gmail.com

Abstract-Characterizing the time variations of signals emitted by mobile terminals provides complementary information to health authorities, especially with the increase of frequency and energy of radiation towards millimeter waves. This experimental work aimed to quantify and classify the time variability of the electric field level measured at 10cm from a mobile phone connected sequentially to a 4th and 5th generation mobile network. Statistic analysis was performed on data from real-time spectrum analyzers, while self-similarity was computed by first recurrence plots of the radiated emissions, corresponding to five different types of mobile applications. Moreover, specificities to the communication standard and the type of application were identified.

Keywords-human exposure; 5G NR; LTE; mobile phone; field variability

I. INTRODUCTION

Massive mobile phone use has led to a tremendous data traffic increase in wireless networks. The fifth-generation (5G) of mobile communication technology, called New Radio (NR), has been proposed and developed to provide sufficient data speeds [1-2], as the 4th generation (4G) reached its limits. The core features of 5G technology are low communication latency, higher download speeds, higher cell density, ultrareliability, etc. [3]. Compared to the 4G mobile communication standard, called Long Term Evolution (LTE), that uses frequencies lower than 6GHz [4], the 5G NR standard uses two sets of frequency ranges: Frequency Range F1 (FR1) [5] has a maximum of 6GHz and an extension up to 7.125GHz, and Frequency Range F2 (FR2) from 24.25 to 52.60GHz [6]. The spread of such technologies has raised continuous public worries about the associated health risks. This study aims to examine and compare the time-variability of the radiated emissions on these networks.

4G LTE involves the use of Orthogonal Frequency-

Division Multiplexing (OFDM) and Single Carrier-Frequency Division Multiple Access (SC-FDMA) for downlink (DL) and uplink (UL) transmissions respectively [7]. Two frame types are delivered [8]: type 1 uses Frequency Division Duplex (FDD), while type 2 uses Time Division Duplex (TDD). In FDD mode, the 4G frame has a duration of 10ms and contains 10 subframes or 20 slots. In TDD mode, the frame has the same duration but is divided into 2 halves of frames with a length of 5ms. The minimum resource that can be used in UL and DL is called Resource Block (RB), which lasts 0.5ms, occupies 180kHz, and contains 12 subcarriers with a spacing of 15kHz [9]. The number of subcarriers and symbols differ for each RB, depending on the length of the cyclic prefix and the spacing of the subcarriers. The slots consist of 6 OFDM symbols in an extended cyclic prefix and 7 symbols in a normal cyclic prefix. 5G NR adopts, similar to 4G, the FDD and TDD techniques, while the signals are OFDM modulated. 5G uses a grid structure consisting of subcarriers in the frequency domain and OFDM symbols in the time domain [10]. For services requiring low latency and high frequencies, 5G supports subcarrier spacings of 30, 60, 120, and 240KHz, based on the subcarrier of 15kHz, whereas the subcarrier spacing in 4G is 15KHz [11]. In the time domain, OFDM symbols are used to construct slots, subframes, and frames. A frame is 10ms long and consists of 10 subframes. In the extended cyclic prefix, a slot consists of 12 OFDM symbols, while in the case of a normal cyclic prefix a slot consists of 14 symbols [12]. In the frequency domain, RB consists of 12 consecutive subcarriers. The access in 5G is based on a procedure that involves the detection of the Synchronization Signal (SS). Similarly to 4G, the SS in 5G consists of two signals: the Primary Synchronization Signal (PSS) and the Secondary Synchronization Signal (SSS). One of the biggest differences between 4G and 5G is that in 5G the SS blocks are transmitted as a directional signal with a high periodicity, while in 4G the Cell-specific Reference Signal (CRS) is distributed in frames

Corresponding author: Delia-Bianca Deaconescu

and is transmitted throughout the cellular network. An SS/PBCH block consists of a Physical Broadcast Channel (PBCH) and De-Modulation Reference Signals [13].

Like in 4G, random access in 5G is performed in 4 steps. At first, the User Equipment (UE) identifies the SSB within the SS Burst Set by using part of the time index carried by the PBCH and transmits a Physical Random Access Channel (PRACH). The 5G standard defines 13 PRACH formats, some with fixed and others with variable subcarrier spacings, that can fit into an NR slot. When a base station uses beamforming and different beams are applied to multiple SS/PBCH block transmissions, PRACH resources are associated with SS/PBCH blocks. In this way, UE transmits a PRACH [14] to randomly initiate the access. Therefore, the base station figures out which SS/PBCH block was received by the UE based on the received PRACH resources. In the next random access procedure, the base station can use transmission/reception beamforming directed to the UE.

A major improvement in 5G networks is the use of active antennas that can synthesize many beams pointing to different directions in continuous dynamic [15-16]. Beamforming is achieved by combining elements in an antenna array. Massive Multiple-Input Multiple-Output (Ma-MIMO) exploits the resources in the space dimension and enables users connected to the same base station to use the same time and frequency resources. This ability is defined by a 3GPP antenna port and is associated with a specific set of signals that allow the reuse of time-space resources of the channel. MIMO transmission is based on two different physical phenomena, polarization multiplexing and spatial multiplexing [17].

With the advent of 5G, one of the concerns of mobile technology users is related to the impact of radiation on human health. As the 5G NR standard is characterized by the use of different technical features (advanced TDD, beam-forming, beam steering, and Ma-MIMO), the classical method of measuring the emitted power density of a mobile device, as applied in 4G, cannot be used as such. In [18], a measurement method was proposed based on the evaluation of extrapolation factors associated with beam sweeping and TDD access mode, which can be used to estimate the instant maximum and the total power transmitted during a 5G radio frame. As 5G systems have unprecedented beam management flexibility, Maximum Permissible Exposure (MPE)-specific measurements are applied in unknown beam states. A solution to solve this problem was proposed in [19] using a beam-forming technique of UEs, concluding that using a UE capable to interact actively with the base station forces the system into a suitable mode for measurement. An Electromagnetic Field (EMF) level estimation technique was proposed in [20], derived from a base station tested in Single-User MIMO (SU-MIMO) coding. The efficiency of using the extrapolation technique for 5G technology was demonstrated. The number of multiplexed subchannels increased by using Multi-User MIMO (MU-MIMO) systems, and the spatial variation of the field could be exploited. This approach expands beam-forming and spatial filtering and allows the reuse of time and frequency resources with a low level of user interference. Optimization of the antenna array to obtain maximum performance in Line-of-Sight

(LoS) propagation condition was explored in [21], introducing a predictor factor for beam-forming losses and a way to use it in MU-MIMO systems. Moreover, grating lobes did not have a negative impact in MU-MIMO systems, while using larger inter-element spacings can be advantageous.

In [22], the first experimental measurement session made in a 5G site was presented. A five-step procedure was applied to assess in-situ the exposure of people due to emissions of 5G base stations. Additional factors such as the temporal duty cycle, the spatial duty cycle, and a TDD factor, were added to the description of the theoretical maximum exposure level following IEC Standard 62232: 2017 [23]. Furthermore, the levels of the E-field per resource element were measured and extrapolated to a theoretical maximum strength, while all reported values were below the ICNIRP reference level [24]. In 5G systems, beamforming may represent a health risk due to the momentary intense increase of the radiated power and the dynamics of these variations. So far, no scientific evidence has been reported to sustain this aspect. Some recent studies reported the possibility of reducing exposure by adopting the beamforming technique [25]. In [26], a scenario was considered to evaluate the impact of pencil beamforming, as a strong reduction in human exposure was observed when the tuning of traffic beams integrated localization information. When the localization uncertainty was lower, the synthesized beams were narrower, and the EMF exposure decreased. As stated above, EMF human exposure from cellular network devices originates from two sources: DL (base stations) and UL (own or a nearby person's handset/terminal). The actual power output of UE is set by the network at the lowest level, while the power transmitted by a base station varies with the area it serves. Over time, small cells increased the network capacities and lowered the power. It is reported that more than 70 million small cells will be installed worldwide by 2025, with one-third belonging to 5G systems [27]. Very few papers quantified the radiation emitted by a mobile terminal in 5G networks [28].

This study aims to highlight the time-variation peculiarities of the radiated field near a UE operating in either a 4G or 5G network. The objective was the comparison of the dynamics of the emitted field strength during the use of several mobile applications types, to expand the knowledge on the variation of the user exposure in time. The dynamics of RF exposure may be important in triggering biological responses at the cell membrane level [29]. Since a new approach is proposed for the increasing frequencies towards millimeter-wave range [30], paving the way to the experimental findings on the time-variability of the emitted radiation may represent a valuable complementary instrument in expo-dosimetry of new mobile technologies.

II. MATERIALS AND METHODS

A Motorola smartphone model g 5G plus (XT 2075-3), connected sequentially to 4G and 5G in FR1, was used as the source of EMF exposure. In both connections, the location of the base station was the same related to the UE, at 75m distance, in non-LOS propagation as UE was located inside a building. The main characteristics of the UL signals (both networks used TDD) were: a) in 4G, the central frequency was $f_1=2.59\text{GHz}$ and the channel bandwidth was $BW_1=20\text{MHz}$, b)

in 5G, the connection used band n77 with central frequency $f_2=3.7\text{GHz}$ and channel bandwidth $BW_2=40\text{MHz}$. UE could deliver a maximum transmitted power of 23dBm for 4G and 5G. A line parallel to the UE upper edge was chosen to capture the radiated electric E-field level in far-field conditions of propagation near the phone, at a 10cm distance, where three E-field probes were located at the same distance between them. The following measuring instruments were used (Figure 1): three identical portable real-time spectrum analyzers type Spectran 5 Aaronia (HF 80120 V5 X model), three small PSB E1 E-field probes connected to the analyzers, and laptops.



Fig. 1. Measurement ensemble with electric field probes, real-time spectrum analyzers, laptops, and the Motorola One 5G phone.

The time-series data of emitted power were synchronously recorded and retrieved using Aaronia RTSA Suite Pro and Aaronia MCS Spectrum Analysis. Five mobile applications were used as sources of the EMF emissions on both networks: video call, voice call, file upload, file download, and streaming. Three measurements (R1, R2, R3) were performed on each mobile application and probe (P1, P2, P3). Each power level stream was recorded continuously for 25s and the sampling periodicity was 100ms. The spectral analyzer was set to a Real-Time Bandwidth Span (RTBW) of 88MHz, for 4G and 44MHz for 5G. After collecting the evolution of the signal spectrum in time, the channel power was calculated every 100ms, by:

$$P_{ch} = \frac{\sum_{f=F\text{ start}}^{F\text{ stop}} 10^{\frac{FFT\ Bin(f)}{10}}}{Wb} \quad (1)$$

where $F\text{ start}$ and $F\text{ stop}$ are the limits of the spectrum in the channel, $FFT\ Bin(f)$ is the power level of each of the spectral components (440 frequency bins were used), and window bandwidth Wb is the resolution bandwidth (195kHz for the 4G and 98kHz for the 5G). Once the power levels were determined, the E-field strengths in air, at 10cm from the UE and their time-evolution was calculated, using the field probe calibration files.

Based on these time series of E-field strength values, the descriptive statistics of field levels per each emission type were calculated and represented in Poincare plots for all 90 situations (5 mobile applications \times 2 communication standards \times 3 field probes \times 3 repetitions). The idea of capturing the self-similarity of the emission dynamics was implemented over the

time series in the form of a two-dimensional recurrence map called Poincare plots, which was applied for the first time in [31] for wireless local area network emissions. Standard descriptors were used to quantify the Poincare ellipse geometry: the ellipse axes, namely SD1 (short-term variability) and SD2 (long-term variability). SD1 represents the standard deviation of the distances of points from axis 1, and SD2 represents the dispersion of points along the axis. The areas of ellipses were calculated to emphasize the differences between the standards, which indicate the total variability and the SD1/SD2 ratios showing the randomness of the time series of the radiated E-field strengths. All the calculations were made to observe the differences in the electromagnetic time-print of the emissions between 4G and 5G.

III. RESULTS AND DISCUSSION

The mean, median and interquartile ranges (IQR) of the E-field strengths, measured in the air at the three points where the probes P1...P3 were situated can be seen in Figure 2. The outliers are represented in the emissions of the 5 mobile applications and can be observed as prominent during streaming and voice calls. Three repetitions are shown for each probe, each of the same color. Figure 2 contains 5 graphs corresponding to each mobile application marked on the abscissa. The first nine boxplots of each graph correspond to 4G, while the second nine correspond to 5G emissions. Upload in 4G presented the largest IQR in which E-field strengths spread. IQR is a measure of the variability around the median, indicating the range of the middle half (50%) of the data. All 4G transmissions during upload, download, and video call showed visible IQR intervals with few outliers. The 5G transmissions on these applications had multiple outliers, indicating that the E-field levels were too far from the central values. Another difference was observed between the 4G and 5G field-level spread for video calls. Voice call and streaming had outliers in both 4G and 5G, indicating that field variability is the highest during such activities. On the other hand, upload and video call in 4G caused more exposure than in 5G. Download and voice call cause lower exposure in 4G, while streaming showed similar exposure levels in both communication standards. However, in these measurements made 10cm from the phone, the field levels were far beyond the ICNIRP safety limits guidelines [24].

Figure 3 shows four characteristic Poincare maps of the time distribution of E-field strength values, measured during video call and file download in 4G and 5G. It can be observed that short-term variability is lower than long-term during an application running in 4G, while the variabilities are vice versa in 5G.

In each network, the radiated field level tends to have a certain scatter pattern for all applications, so the self-similarity in the time variation of the signals depends on the communication standard. Moreover, specificities could be observed between the type of mobile applications. In this sense, Figure 4 shows the ratios between the ellipse axes, the SD1/SD2 ratios, and the average of the results for all probes.

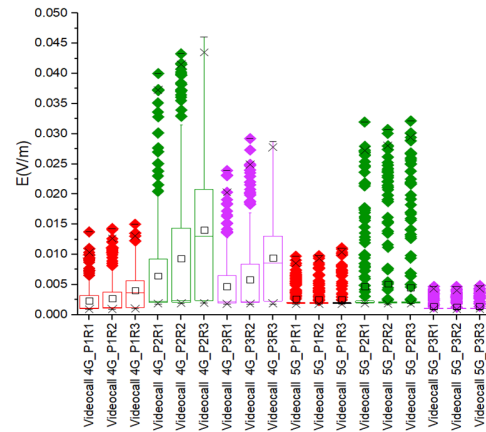
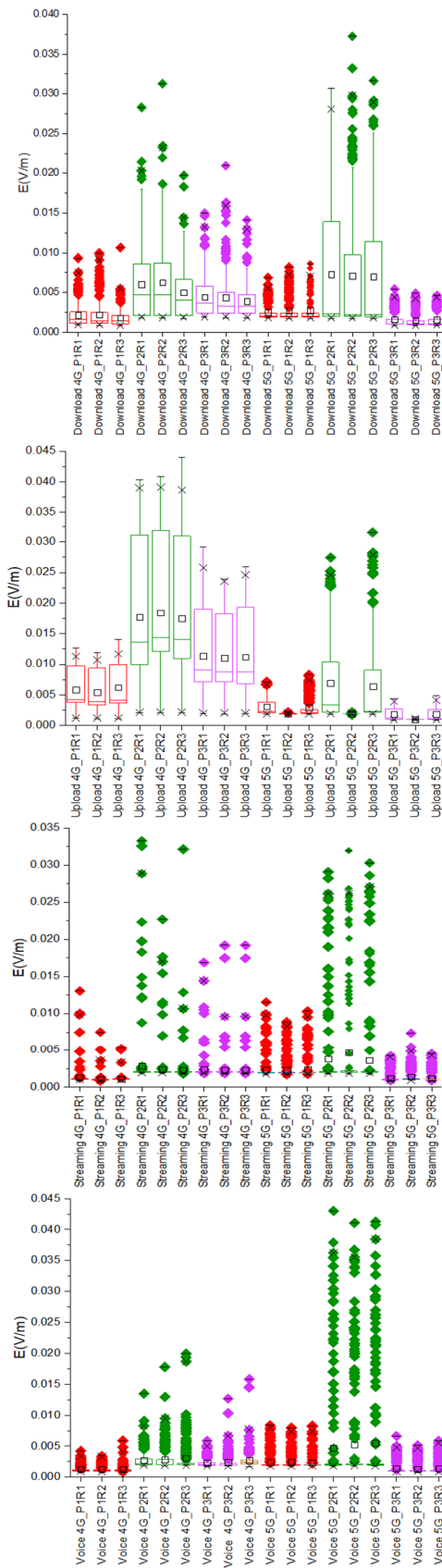


Fig. 2. Boxplots with outliers of E-field strength distributions for all mobile applications, all probes, and repetitions in 4G and 5G networks.

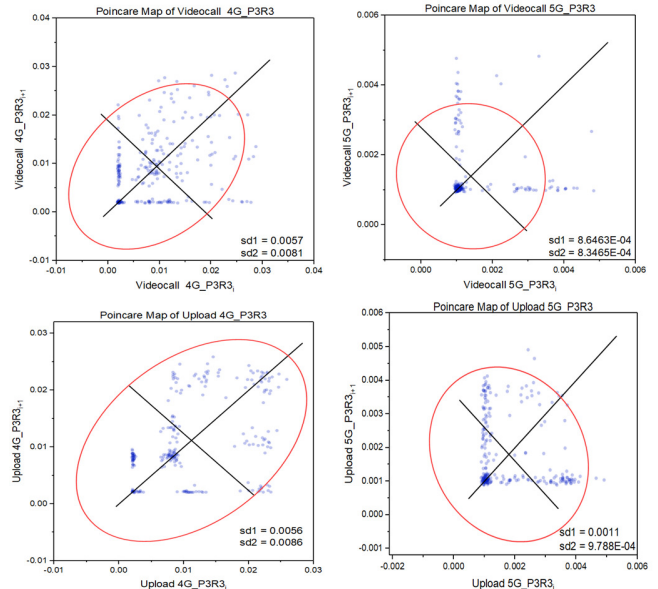


Fig. 3. Poincaré maps of E-field strength near the phone in 4G (left) and 5G standard (right) during two applications.

The results of the ellipse axis ratio for R2 and R3, are presented for the 5 applications on both networks. The lowest ratio between short- and long-time variabilities was found in upload on 4G. The highest ratio between short- and long-time variabilities was found in the 5G download. For all 5G applications, the randomness of the emitted field was higher in the short- than the long-term, as compared to the respective 4G. The Poincaré ellipse areas, shown in Figure 5, indicate that the largest variability of the radiated field corresponds to file upload and video call in 4G. Figure 5 indicates the average areas for two repetitions of the measurements. The total variabilities of the emitted fields were higher in 5G than in 4G for file download, streaming, and voice call. However, upload and video call in 4G had at least one order of magnitude larger variability than the other applications in both standards. As this specific feature confirms that file upload and video call led to the highest exposure levels in 4G, as deduced from Figure 2, it

can be concluded that these applications could be the most interesting for further biological dosimetry research. In 5G, the largest variabilities of the radiated field were observed for voice calls and file download. These high variabilities may be due to the higher field levels in 5G for these two mobile applications. Therefore, at least voice calls deserve special attention in future dosimetric studies devoted to the biological effects of 5G signals.

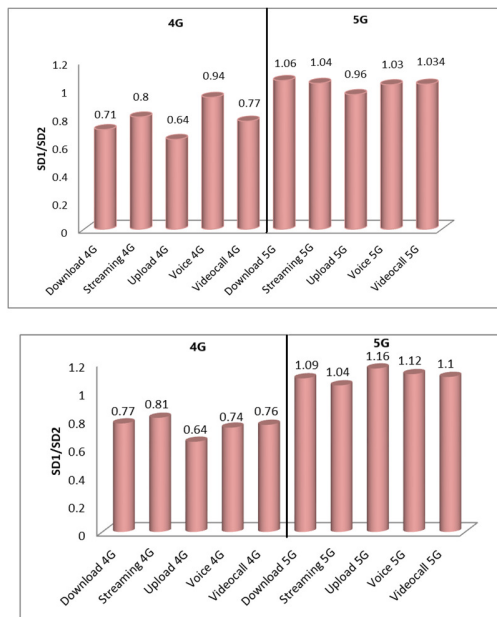


Fig. 4. Average ratios SD1/SD2 of E-field strength ellipses for all mobile applications in 4G and 5G in two repetitions: R1 (up), R2 (down).

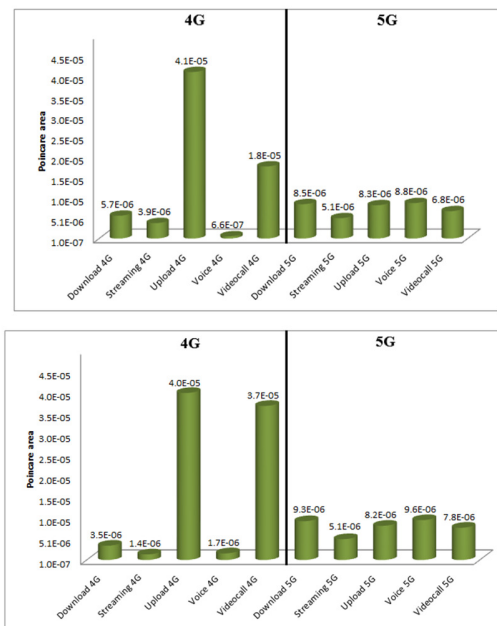


Fig. 5. Areas of the Poincare maps of E field strength for all applications in 4G and 5G in two repetitions: R1 (up), R2 (down).

Previous findings, extracted by applying a different methodology but still based on real-time spectrum analyzers and small and sensitive field probes, emphasized specific features of the time variability of signals emitted by a 4G phone [28]. In line with those findings, this study allowed a step further in extracting the main peculiarities of the time dynamics of the emitted radiation, by comparing the 4G and 5G sub-6 GHz band networks using the same phone model. The novelty of this research was the approach of a complementary characterization of human exposure by the energy fluence rate adapted to the GHz frequency range. Based on this quantity, it was shown that a prediction is possible based on differentiating chaotic behavior from true randomness of 4G and 5G emitted signals evoked by recurrence quantification.

IV. CONCLUSIONS

This study aimed to identify the differences in the time variability of signals emitted by a mobile phone when sequentially connected to a 4G-LTE or 5G-NR network. The main reason behind this study was the need of describing not only the dose of radiation absorbed by a human body while using a phone but also the average or the momentary dose rate. While the present safety exposure standards do not yet expressly require such knowledge, increasing the frequency towards tens of GHz in 5G networks means an increase in the energy of the radiation so it might need a time-dependent description similar to the ionizing radiation. Moreover, the averaging time used to describe the biological impact of the field is also very important to accurately describe the safety of people exposed to very short and quasi-stochastic pulses [31].

By experimentally determining the E-field strength variation during the 25s usage of 5 different mobile communication activities in either 4G or 5G networks, which allowed TDD technique and respectively had 20 and 40MHz bandwidths for the transmission, streams of 250 field values were gathered and treated as time-series. The boxplot representations of these data allowed obtaining descriptive statistic distributions, while the Poincare plots showed self-similarity by first recurrence means. The results showed that: a) more intensive dynamics are encountered generally in 5G UL signal than in 4G, b) the time variability is dependent not only on the communication standard but also on the type of mobile application used, c) short-term variability is lower than long-term when using a 4G application, as compared to 5G where the short-term variability of field level is higher than the long-term, d) the lowest ratio between short- and long-time variabilities was encountered for file upload in 4G, while the highest ratio was encountered for file download in 5G, and e) the largest total variabilities in 4G were associated to upload and video call, while in 5G they were noted during voice call and file download. These results provide important knowledge that completes the picture of amplitude-time variation of human exposure to near-the-body used mobile devices.

REFERENCES

[1] S. Parkvall, E. Dahlman, A. Furuskar, and M. Frenne, "NR: The New 5G Radio Access Technology," *IEEE Communications Standards Magazine*, vol. 1, no. 4, pp. 24–30, Dec. 2017, <https://doi.org/10.1109/MCOMSTD.2017.1700042>.

- [2] T. S. Rappaport *et al.*, "Millimeter Wave Mobile Communications for 5G Cellular: It Will Work!," *IEEE Access*, vol. 1, pp. 335–349, 2013, <https://doi.org/10.1109/ACCESS.2013.2260813>.
- [3] F. Rinaldi, A. Raschella, and S. Pizzi, "5G NR system design: a concise survey of key features and capabilities," *Wireless Networks*, vol. 27, no. 8, pp. 5173–5188, Nov. 2021, <https://doi.org/10.1007/s11276-021-02811-y>.
- [4] H. Singh, N. Mittal, A. Gupta, Y. Kumar, M. Woźniak, and A. Waheed, "Metamaterial Integrated Folded Dipole Antenna with Low SAR for 4G, 5G and NB-IoT Applications," *Electronics*, vol. 10, no. 21, Jan. 2021, Art. no. 2612, <https://doi.org/10.3390/electronics10212612>.
- [5] "ETSI TS 138 101-1 V15.3.0 (2018-10) 5G; NR; User Equipment (UE) radio transmission and reception; Part 1: Range 1 Standalone (3GPP TS 38.101-1 version 15.3.0 Release 15)," ETSI, France, RTS/TSGR-0438101-1v30, Oct. 2018.
- [6] "ETSI TS 138 101-2 V15.3.0 (2018-10) 5G; NR; User Equipment (UE) radio transmission and reception; Part 2: Range 2 Standalone (3GPP TS 38.101-2 version 15.3.0 Release 15)," ETSI, France, RTS/TSGR-0438101-2v30, Oct. 2018.
- [7] D. QingXia, D. Gang, and C. HaiYan, "Research on Key Technology of TD-LTE Standard 4G Mobile Communications Network," *The Open Cybernetics & Systemics Journal*, vol. 9, no. 1, Sep. 2015.
- [8] S. Tabbane, "4G to 5G networks and standard releases," Bangkok, Thailand, Oct. 2019.
- [9] F. Schaich and T. Wild, "Subcarrier spacing - a neglected degree of freedom?," in *2015 IEEE 16th International Workshop on Signal Processing Advances in Wireless Communications (SPAWC)*, Jun. 2015, pp. 56–60, <https://doi.org/10.1109/SPAWC.2015.7226999>.
- [10] "The 3GPP Specification series TS. 38," 3GPP, France, 2017.
- [11] D. Franci *et al.*, "Experimental Procedure for Fifth Generation (5G) Electromagnetic Field (EMF) Measurement and Maximum Power Extrapolation for Human Exposure Assessment," *Environments*, vol. 7, no. 3, Mar. 2020, Art. no. 22, <https://doi.org/10.3390/environments7030022>.
- [12] H. Keller, "On the Assessment of Human Exposure to Electromagnetic Fields Transmitted by 5G NR Base Stations," *Health Physics*, vol. 117, no. 5, pp. 541–545, Nov. 2019, <https://doi.org/10.1097/HP.0000000000001089>.
- [13] Y. Kryukov, D. Pokamestov, and E. Rogozhnikov, "Cell search and synchronization in 5G NR," *ITM Web of Conferences*, vol. 30, 2019, Art. no. 04007, <https://doi.org/10.1051/itmconf/20193004007>.
- [14] E. G. Larsson, O. Edfors, F. Tufvesson, and T. L. Marzetta, "Massive MIMO for next generation wireless systems," *IEEE Communications Magazine*, vol. 52, no. 2, pp. 186–195, Feb. 2014, <https://doi.org/10.1109/MCOM.2014.6736761>.
- [15] H. Alsaif, "Extreme Wide Band MIMO Antenna System for Fifth Generation Wireless Systems," *Engineering, Technology & Applied Science Research*, vol. 10, no. 2, pp. 5492–5495, Apr. 2020, <https://doi.org/10.48084/etasr.3413>.
- [16] D. T. T. My, H. N. B. Phuong, T. T. Huong, and B. T. M. Tu, "Design of a Four-Element Array Antenna for 5G Cellular Wireless Networks," *Engineering, Technology & Applied Science Research*, vol. 10, no. 5, pp. 6259–6263, Oct. 2020, <https://doi.org/10.48084/etasr.3771>.
- [17] S. Ghnimi, A. Nasri, and A. Gharsallah, "Study of a New Design of the Planar Inverted-F Antenna for Mobile Phone Handset Applications," *Engineering, Technology & Applied Science Research*, vol. 10, no. 1, pp. 5270–5275, Feb. 2020, <https://doi.org/10.48084/etasr.3287>.
- [18] D. Franci *et al.*, "An Experimental Investigation on the Impact of Duplexing and Beamforming Techniques in Field Measurements of 5G Signals," *Electronics*, vol. 9, no. 2, Feb. 2020, Art. no. 223, <https://doi.org/10.3390/electronics9020223>.
- [19] M. D. Migliore *et al.*, "A New Paradigm in 5G Maximum Power Extrapolation for Human Exposure Assessment: Forcing gNB Traffic Toward the Measurement Equipment," *IEEE Access*, vol. 9, pp. 101946–101958, 2021, <https://doi.org/10.1109/ACCESS.2021.3092704>.
- [20] S. Adda *et al.*, "A Theoretical and Experimental Investigation on the Measurement of the Electromagnetic Field Level Radiated by 5G Base Stations," *IEEE Access*, vol. 8, pp. 101448–101463, 2020, <https://doi.org/10.1109/ACCESS.2020.2998448>.
- [21] D. Pinchera, M. D. Migliore, and F. Schettino, "Optimizing Antenna Arrays for Spatial Multiplexing: Towards 6G Systems," *IEEE Access*, vol. 9, pp. 53276–53291, 2021, <https://doi.org/10.1109/ACCESS.2021.3070198>.
- [22] S. Aerts *et al.*, "In-situ Measurement Methodology for the Assessment of 5G NR Massive MIMO Base Station Exposure at Sub-6 GHz Frequencies," *IEEE Access*, vol. 7, pp. 184658–184667, 2019, <https://doi.org/10.1109/ACCESS.2019.2961225>.
- [23] "Determination of RF field strength, power density and SAR in the vicinity of radiocommunication base stations for the purpose of evaluating human exposure," IEC, Switzerland, IEC 62232:2017, Nov. 2019.
- [24] International Commission on Non-Ionizing Radiation Protection (ICNIRP), "Guidelines for Limiting Exposure to Electromagnetic Fields (100 kHz to 300 GHz)," *Health Physics*, vol. 118, no. 5, pp. 483–524, May 2020, <https://doi.org/10.1097/HP.0000000000001210>.
- [25] *5G and Health*. Wellington, New Zealand: Ministry of Health, 2019.
- [26] L. Chiaraviglio *et al.*, "Planning 5G Networks Under EMF Constraints: State of the Art and Vision," *IEEE Access*, vol. 6, pp. 51021–51037, 2018, <https://doi.org/10.1109/ACCESS.2018.2868347>.
- [27] "The impact of RF-EMF exposure limits stricter than the ICNIRP or IEEE guidelines on 4G and 5G mobile network deployment," ITU - T, Switzerland, Series K-Supplement 14, May 2018.
- [28] S. M. and P. Bechet, "Non-Stationary Statistics with Amplitude Probability Density Function for Exposure and Energy Density Reporting Near a Mobile Phone Running 4G Applications," *Progress In Electromagnetics Research M*, vol. 89, pp. 151–159, 2020, <https://doi.org/10.2528/PIERM19110706>.
- [29] M. Simkó and M.-O. Mattsson, "5G Wireless Communication and Health Effects—A Pragmatic Review Based on Available Studies Regarding 6 to 100 GHz," *International Journal of Environmental Research and Public Health*, vol. 16, no. 18, Jan. 2019, Art. no. 3406, <https://doi.org/10.3390/ijerph16183406>.
- [30] E. Neufeld, T. Samaras, and N. Kuster, "Discussion on Spatial and Time Averaging Restrictions Within the Electromagnetic Exposure Safety Framework in the Frequency Range Above 6 GHz for Pulsed and Localized Exposures," *Bioelectromagnetics*, vol. 41, no. 2, pp. 164–168, 2020, <https://doi.org/10.1002/bem.22244>.
- [31] S. Miclaus, A. Sarbu, and P. Bechet, "Using Poincare Plots for Feature Extraction of the Dynamics of Electromagnetic Field Exposures when Using Different Protocols of Wi-Fi Communications," in *2021 8th International Conference on wireless communication and sensor networks*, New York, NY, USA, Jan. 2021, pp. 32–38, <https://doi.org/10.1145/3461717.3461723>.